6.4

A NEW NARROWBEAM, MULTI-FREQUENCY SCANNING RADIOMETER AND ITS APPLICATION TO IN-FLIGHT ICING DETECTION

David J. Serke[*]
National Center for Atmospheric Research, Boulder, Colorado

Paul Beaty
Radiometrics Corporation, Boulder, Colorado

Andrew L. Reehorst
NASA Glenn Research Center, Cleveland Ohio

Pat Kennedy
Colorado State University, Fort Collins, Colorado

Fred Solheim and Randolph Ware
Radiometrics Corporation, Boulder, Colorado

Marcia K. Politovich
National Center for Atmospheric Research, Boulder, Colorado

David Brunkow and Robert Bowie
Colorado State University, Fort Collins, Colorado

1. INTRODUCTION

Aircraft accrete ice in flight when the aircraft's surface impacts supercooled liquid water. Accretion often occurs on engine intakes or propellers, leading edges of the wings and tail fin structures. This in-flight icing can result in significant loss of aerodynamic performance due to increased drag, change in the effective wing shape and added weight. Loss of performance can lead to dangerous aircraft responses that are outside of the envelope of normal flight operations. It is an ongoing goal in the aviation safety community to be able to accurately quantify in time and space, the presence of in-flight icing hazards. Since aircraft icing is a process that requires the presence of an aircraft to occur, icing cannot be directly measured with a remote system. While ideally all aircraft would be equipped with icing remote detection equipment to provide coverage over their entire flight paths, this is not practical. The need to provide a ground-based capability that can provide information to all aircraft entering and departing a terminal area is a key element in facilitating icing avoidance.

The current techniques for the remote detection and measurement of icing conditions rely on the identification of liquid water and then the inference or measurement of the surrounding air temperature. The Current Icing Product (CIP), developed by the National Center for Atmospheric Research (Bernstein et al., 2005), ingests near-realtime Rapid Update Cycle model atmospheric and microphysical fields, visible and infrared satellite data, surface weather observations, PIlot REPorts (PIREPs) and lightning network data to infer liquid and subfreezing temperatures aloft. CIP is

an operational system currently in use by the FAA. Another warning system is the NASA Icing Remote Sensing System (NIRSS), which is a testbed prototype (Reehorst et al., 2006). It consists of a vertically pointing Metek K-band radar to define cloud top and base heights and to determine cloud layer structure. There is also a Radiometrics Corporation multi-channel radiometer (Solheim et al., 1998), whose channels are used to derive integrated liquid water and atmospheric temperature profiles. A laser ceilometer is also incorporated to further define the cloud base. Software integrates the data streams in realtime and the derived liquid is distributed within the detected cloud layer(s) based on internal logic to arrive at an in-flight icing hazard categorization. This testbed system is an effort to provide in-flight icing hazard warnings with existing, cost-effective technologies and the system is currently positioned near John Hopkins Airport at NASA Glenn Research Center in Cleveland, Ohio.

Combining ground-based microwave radiometers with radars has shown great promise, but deficiencies with the current generation of radiometers have somewhat limited their value. These shortcomings include a wide beamwidth (typically 6^0), which limits the resolution and possibility of directly comparing the data to the 1^0 beamwidth available with weather radars. In our Phase I effort, we have determined solutions to several technical challenges with the design of a new instrument -- the NASA Narrow beam, Multi-waveband Scanning Radiometer (NNMSR) that is to operate in concert with weather radars. This report will detail the design (section 2.1), calibration (section 2.2), overview of NNMSR channel data interpretation (section 3) and field testing of the NNMSR at Colorado State University's polarized CHILL S-band radar facility (Figure 1, section 4) for the application of improving in-flight icing hazard detection. This new sensor, when integrated into the existing NIRSS system and positioned near the soon-to-be-polarized NEXRAD

*Corresponding author address: David J. Serke,
National Center for Atmospheric Research,
3450 Mitchell Lane, Boulder, CO 80301;
Email: serke@ucar.edu

radars near each large national terminal, can fulfill the need for airport terminal area icing hazard warnings.

There are other possible applications of this new system beyond terminal area in-flight icing hazard detection that should be mentioned. The system could help nowcast the need for (or lack of need for) the application of deicing solutions in advance of departure, creating savings and reducing delays. The system could also provide valuable high resolution mesoscale meteorological inputs for weather and climate model initializations (Fabry and Meunier, 2009). The current research is only related to in-flight icing applications, however, and no other applications are being pursued as part of this work.

2. SYSTEM REALIZATION

2.1 Design

The NNMSR project began when the Boulder, CO based Radiometrics Corp. applied for and received a Small Business Innovation contract in 2004 to design and construct a turnkey, fast- sampling, multi-frequency, dual polarization narrowbeam radiometer system. The specified system was to include 21 channels in the K-band, and a separate W-band receiver. With its broad K-band sampling capability, it can integrate water vapor along the beam and provide information on the discrimination of liquid and ice phase hydrometeors utilizing the W-band polarization. By using data from both bands, liquid water path can be derived. The system also employs a fast beam steering system to operate in concert with a weather radar. Adding to these measurement capabilities the system's full elevation and azimuth scanning capability results in a measurements with the potential of providing terminal area icing detection and warning. The importance of the technology described in this work is that the value of important radiometric observations provided by the NNMSR are greatly enhanced by matching the sample volume of research radars.

The K-band (20-30 GHz) receiver was chosen for inclusion in the NNMSR because the band includes the peak and shoulder of a water vapor absorption line. By comparing the received brightness temperatures (TB) from a channel near the peak of the water absorption line to a second channel in the water vapor window region, values for integrated water vapor and integrated cloud liquid water can be obtained. This is because channels near the peak of the water vapor absorption line have an absorption coefficient for water vapor that is nearly independent of altitude. Channels well away from the water absorption peak are used because the received TB is dominated by the absorption and emission from liquid water (which increases with the frequency squared).

The W-band 89 GHz channel, is sensitive to cloud liquid water but is also strongly effected by scattering from precipitation sized glaciated hydrometeors (Troitsky et al. 2003). For this reason, the

Figure 1: Image of the NNMSR located at the CSU CHILL radar site during the summer of 2009.

Parameter	NASA Narrowbeam Multi-channel Scanning Radiometer (NNMSR)
Frequency Channels (GHz)	22.000, 22.234, 22.500, 23.000, 23.034, 23.500, 23.834, 24.000, 24.500, 25.000, 25.500, 26.000, 26.234, 26.500, 27.000, 27.500, 28.000, 28.500, 29.000, 29.500, 30.000 and 89.0 V and 89.0 H
Antenna Beamwidth ($^{\circ}$)	1
Calibration	Tipping curve, Microwave absorber at ambient temperature and LN_2
Mass	Scanhead ~ 90 kg, Tripod ~ 16 kg
Dimensions	Scanhead 1mx1mx1.5m, Tripod 3mx3mx2m
Power Consumption	110 V

Figure 2: Parameters of the NNMSR system.

W-band receiver was separated into vertically and horizontally polarized receiver channels to attempt to discriminate cases when horizontally oriented glaciated particles were present.

2.2 Calibration

Figure 2 details relevant parameters and calibration procedures employed in the development of the operational NNMSR system. In the resulting passive radiometer system, all beams are collinear and match the antenna gain pattern of NEXRAD and weather research radars. Elevation and azimuth beam matching between the K and W band radiometers was achieved by scanning a 1^0 by 1^0 grid encompassing the tallest peaks on the Front Range near Boulder, Colorado. These peaks were located approximately 7 km in distance from the radiometer. Many hours of vertical and horizontal profiles across these mountain targets were averaged and analyzed so that precise vertical and horizontal beam matching was achieved.

3. DATA INTERPRETATION

Lohnert and Crewell (2003) used a large radiosonde profile dataset to model clouds in three different cloud models, which all used a modified adiabatic assumption and a threshold for relative humidity. They developed nine different regression algorithms of LWP for multi-frequency ground-based radiometers and applied them to data sets where clouds were generated by the threshold method, gradient method and a cloud microphysical model. The generalized form of the retrieval is

$$LWP = c_0 + \mathbf{c}*\mathbf{TB} \qquad (1)$$

where $\mathbf{c}$ is the coefficient vector with dimensions defined by the number of frequencies of brightness temperatures as a vector, $\mathbf{TB}$, used in the retrieval. For this study, a LWP algorithm was selected for use based on availability and proximity of NNMSR channels to those in the reference publication, shown as

$$LWP= c_0 -7.5*TB_{23.0} + 6.6*TB_{28.5} + 4.5*TB_{90.0} \quad (2)$$

which had an RMS of 19.8 gm^{-2} and a COR^2 of 0.96 between the modeled and retrieved LWP. In their study, they found that the inclusion of the W-band channel made a significant improvement in the LWP correlation statistics. For the case studies in the following section, we will compute the LWP in this fashion as part of the analysis.

It is important to note that liquid water on the radiometer dish can result in artificially high values of brightness temperature. None of the cases explored in the following sections involved precipitation reaching the surface.

4. CASE STUDIES

Two case studies are discussed in this section which elucidate how the new NNMSR system can be utilized in concert with polarized S-band radars to detect in-flight icing hazards in the airport operational environment.

4.1 September 21st, 2009

The first case study is from September 21st, 2009 when a cold front moved southward from Canada over the CHILL site. The progression of the front can be seen in Figure 3a, as wind barbs from the north below 700 mb, and in 3b as a cooling of the ambient temperature Ta in the atmospheric profile up to 400 mb and a deepening of the northerly wind layer. By the later time period, there is a slight drying of the lowest levels, but a moistening from 3.5 to 6.5 km AGL. The more dense cold air sliding southward behind the front is drying the lowest levels due to it's continental origin. At the same time the lower-level airmass is providing just enough lift to the airmass above it that the upper airmass is becoming saturated and supercooled cloud
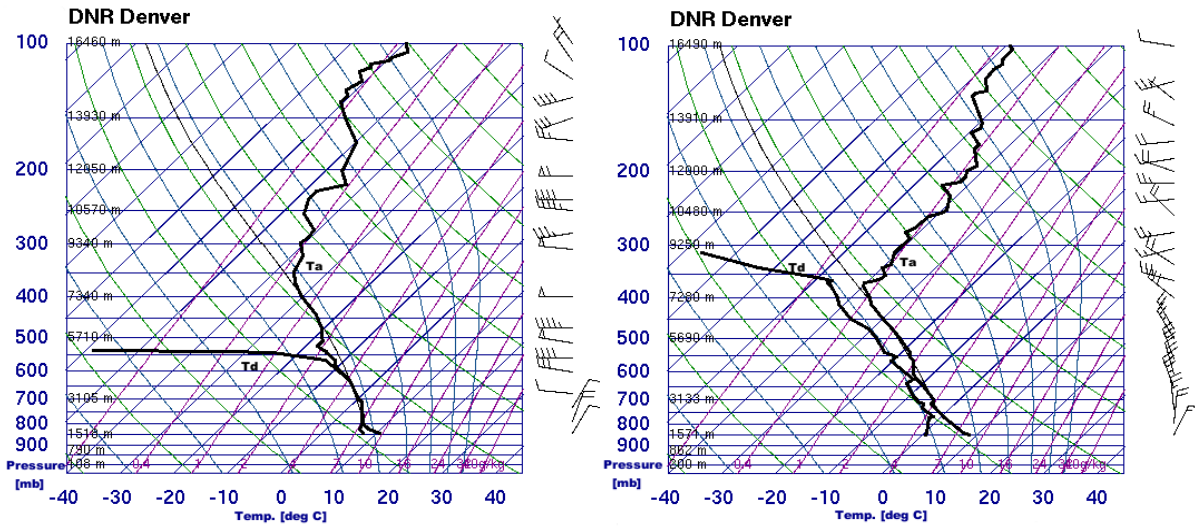
A)   **B)**

Figure 3.   Atmospheric profiles of ambient temperature(Ta) and dewpoint temperature (Td) from 12Z on September 21st (A) and from 00Z on September 22nd (B) from Denver, CO.
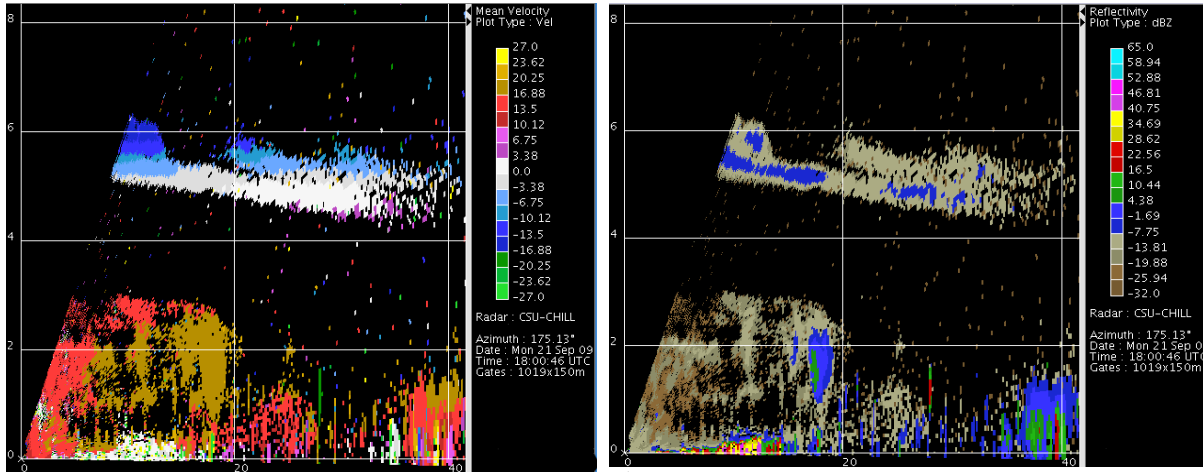
A)   **B)**

Figure 4.   CHILL RHI views from 175° azimuth of radial velocity (A, [ms-1]) and reflectivity (B, [dBZ]) at 18:00Z on September 21st. Vertical and horizontal ranges are in kilometers.
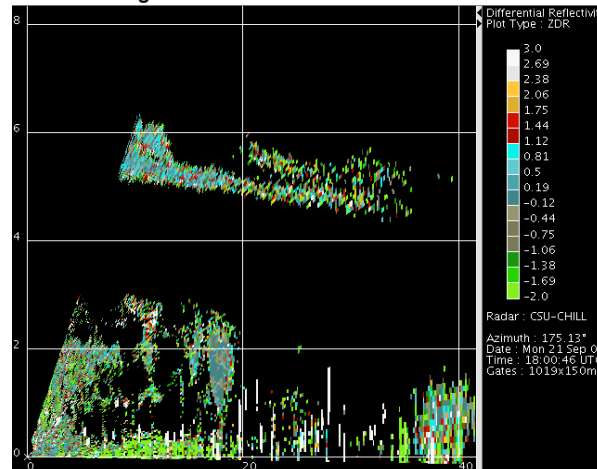
Figure 5.   CHILL RHI views from 175° azimuth of differential reflectivity [dBZ] at 18:00Z on September 21st.

A)   **B)**
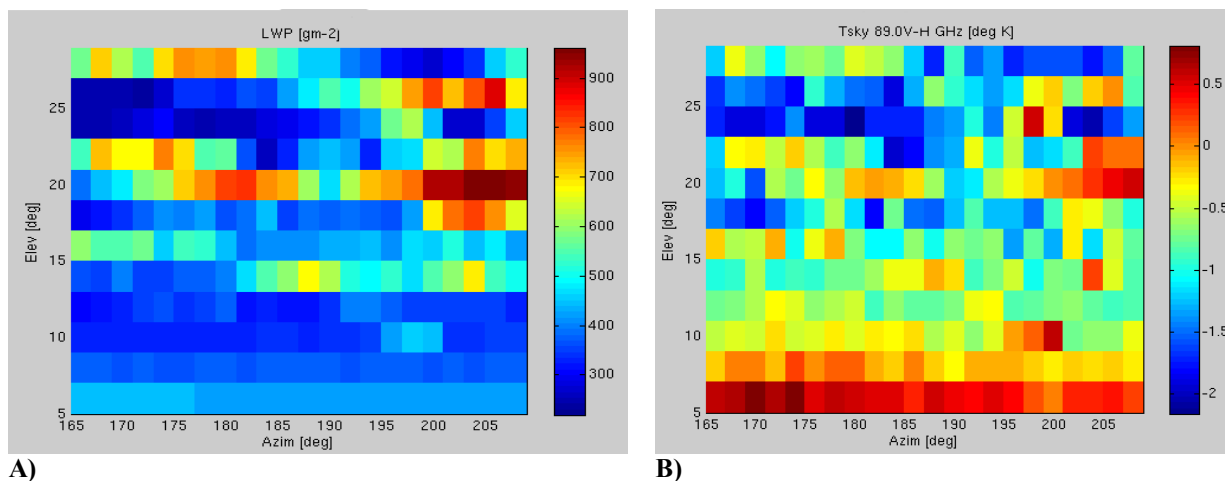
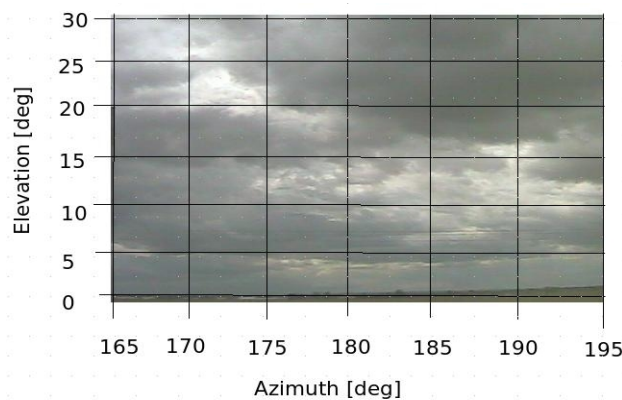*Figure 6. NNMSR derived LWP (A, [gm-2]), 89 GHz V-H (B, °K) at 18:04 Z.*

Figure 7. Visual sky sector image at 18:04 Z.

droplets are forming.   We know this to be true because this time corresponds to when four 'moderate' and one 'light' icing PIREP were reported within one hour and one-hundred nautical miles of the CSU CHILL instrument site. All of these PIREPs were reported in the layer between 4 and 8 km in altitude. The freezing level lowers from 1.6km to 0.9 km by 00Z on September 22nd. No precipitation reached the ground at any time during the times encompassing this case study.

We'll begin by looking at the CHILL moment data and NNMSR derived LWP and 89 GHz polarization differences around 18:00 Z on September 21st. All of the radar data imagery presented in this work are from range-height indicator (RHIs) scan format from 1 to 30⁰ beam elevations, which means the radar was viewing vertical slices of the atmosphere at a fixed azimuth. The signal in the radar velocity field (Figure 4a) supports the synoptic view of a cold front affecting the radar site. Red and orange radial velocity values from the surface up to 3 km indicate flow away from the radar, and since the radar is pointed southward (175° azimuth) this lower layer is the cold, dense airflow from the north behind the cold front. Blueish values in the layer between 4

and 7km altitude have a flow component from the south. Very low reflectivity values below zero dBZ (Figure 4b) in the layer between 4 and 7 km are consistent with findings in previous research (Serke et al., 2008) as an indicator to the presence of supercooled liquid in winter. The differential reflectivity (ZDR, Figure 5a) is a ratio of the returned vertically and horizontally polarized signals and gives some information on the shape and orientation of the dominant particles being viewed by the radar. In the layer between 4 and 7 km where the icing PIREPS are being reported, ZDR values are slightly positive. Values from zero to slightly positive indicate the vertical and horizontal axial dimensions of the targets in the viewing volume are similar, which is consistent with rounded particles. The LWP field was derived for 18:04 Z (Figure 6a) as shown in equation 2. Since NNMSR in its current form is unable to range liquid, it helps to think of this image as a sector of sky centered on due south (180° azimuth) where each pixel is a range integrated measurement of LWP. The supercooled liquid, which is detected otherwise as numerous positive icing PIREPs, show up in this plot as horizontal streaks of elevated LWP in excess of 600 gm-2. The horizontal 'streakiness' is likely due to the passage of super-cooled liquid pockets across the viewed sky sector in the 14 minutes it took to collect all the NNMSR channel data for the sky sector. The visual

view of the same sky sector (Figure 7) comes from a webcam positioned on an instrument tower right next to the NNMSR and depicts a grey, stratiform cloud deck with occasional gaps. The 89 GHz channel was included as part of this system because not only is this band sensitive to emission from liquid water, but it is also effected by the reflection and scattering of microwave radiation from glaciated particles. Oblate ice particles such as dendrites tend to fall with their long axis horizontal. Radiation that is absorbed and emitted is naturally unpolarized (Figure 8), thus the only way to receive a polarized signal is if the particle mass effectively polarizes the signal. This is theorized to occur in the presence of oblate crystals (or large rain drops) as horizontal radiation is preferentially reflected from the surfaces of all the particles at the given viewing angle. When the horizontal component is larger than the vertical, V-H is negative. This is the case in figure 6b for areas where LWP values are smallest. At elevations and azimuths where LWP is largest, 89 V-H is near zero which is consistent with viewing round liquid particles which emit unpolarized radiance. At elevation angles of $5°$ and below,

channel values can be suspect due to surface effects (Troitsky et al., 2003). Quick calculations based on 800 gm^{-2} of LWP (from Figure 6a) distributed through the upper cloud layer with a path length of 1500m (from Figure 4b) at a $20°$ slant angle leads to a significant liquid water content of 0.4-0.5 gm^{-3} through the cloud depth. This significant level of liquid water content is producing the local reports of moderate in-flight icing.

Four hours later at 22:00Z, there were no reported icing PIREPs within one hour and one-hundred nautical miles of the CHILL instrument site. Both the radar and radiometer were operating in the same respective modes of viewing RHIs along $175°$ azimuth for CHILL and a similar southern-facing sky sector for the NNMSR. The change in radar and radiometer signals from the earlier icing time period is dramatic. The radial velocity (Figure 9a) field shows consistent flow from the north from the cloud base at 1km AGL up to 5km altitude. This is again consistent with a deepening layer of cold air flowing southward after a cold frontal passage. The reflectivity RHI (Figure 9b) shows nearly all values are now above 0 dBZ, with the bulk being above 10 dBZ. Streamers of virga are seen reaching downward below
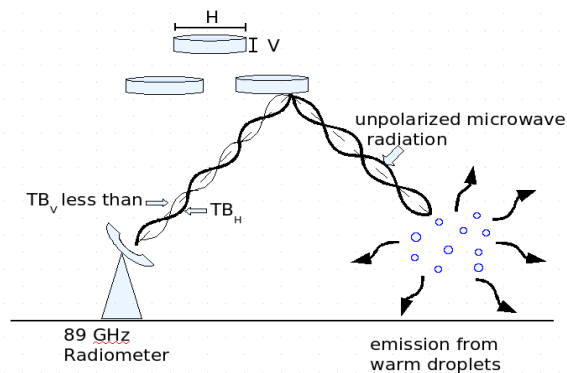

Figure 8. Schematic of unpolarized microwave radiation becoming polarized and how horizontally oriented crystals create TB_V - TB_H < 0.
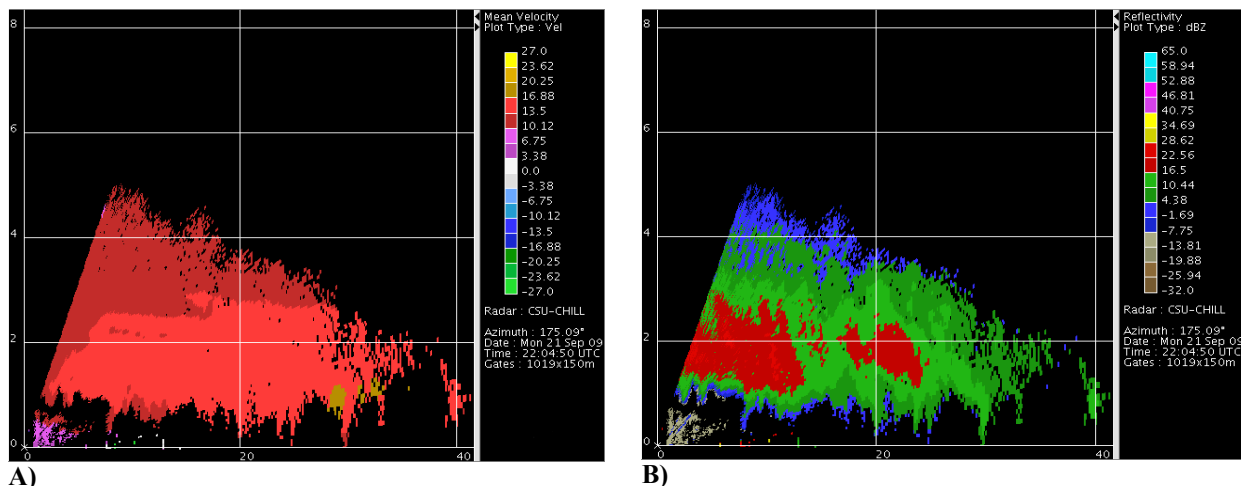

Figure 9. CHILL RHI views from $175°$ azimuth of radial velocity (a, [ms^{-1}]) and reflectivity (b, [dBZ]) at 22:04Z on September 21st.
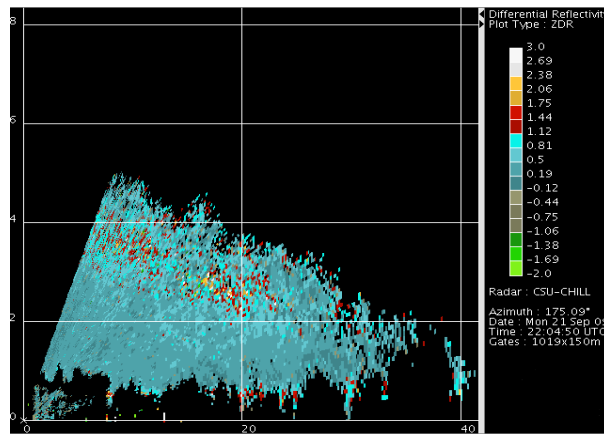
Figure 10.   CHILL RHI views from 175º azimuth of differential reflectivity [dBZ] at 22:04Z on September 21st.
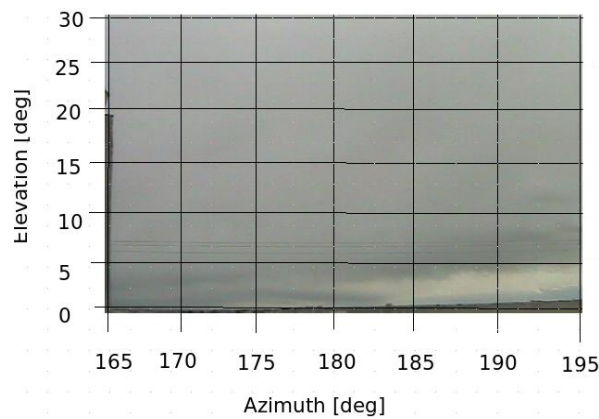

Figure 11.   Gridded visual sky sector image at 22:28 Z on September 21st.

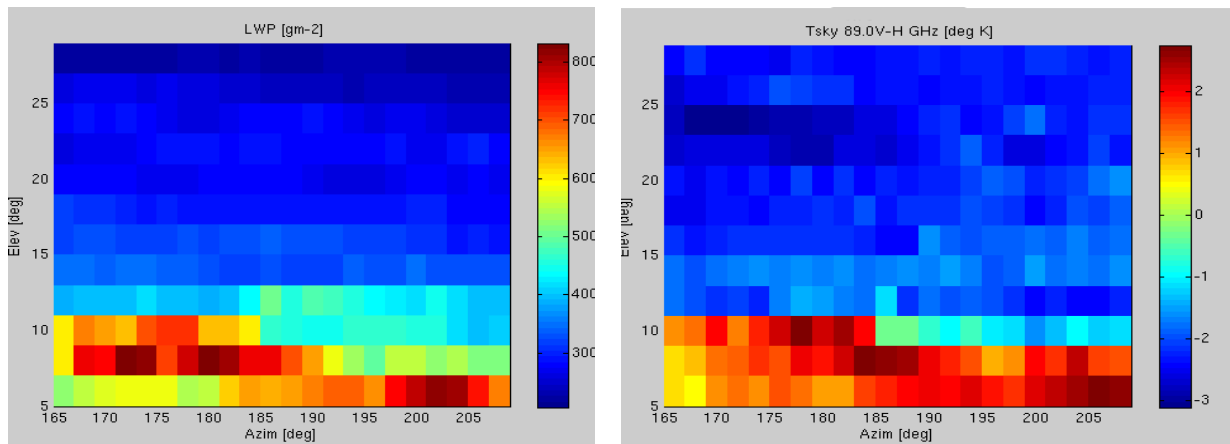**A)**   **B)**

Figure 12.   NNMSR derived LWP (a, [gm-2]), 89 GHz V-H (b, [ºK] at 22:28Z on September 21st.

the clouds, indicating that particles are large and weighty enough to begin falling out of the cloud, but are sublimating before they reach the surface. ZDR values (Figure 10a) are somewhat positive near the cloud base and average about +1 dB near the cloud tops, consistent with small particles that are somewhat oriented. All of these clues from the CHILL moment data lead to the conclusions that the particle

population in this increasingly cold cloud layer has a uniformly high reflectivity and a uniformly consistent shape and/or particle orientation. This particle mass must be almost fully glaciated, which is partially supported by the lack of positive icing PIREPs at a time of day when a significant volume of air traffic was transecting the region.

The south-facing visual sky sector image (Figure 11) shows a grey stratiform cloud deck with no gaps, with

what appears to be blue skies at low elevation angles. Retrieved LWP (Figure 12a) values at angles above 10° are uniformly below 300 gm⁻², which is half to one-third the values seen at the earlier case time. Figure 12b shows negative 2 to 3 degree V-H differences at viewing angles above 10°. This is due to relatively large (warm TB) emission from water droplets in the lower levels of the atmosphere being more preferentially scattered by horizontally oriented ice particles in the horizontal component than the vertical component back towards the passive NNMSR, thus creating a negative V-H channel difference. One curious feature of the LWP and 89 V-H views are the large values of each field below 10° elevation. Troitsky et al., (2003) demonstrated that theoretically calculated polarization differences at 85 GHz became large and positive at low viewing angles in the presence of horizontally oriented oblate particles (such as plates, dendrites or rods). Since the 3 GHz CHILL radar ZDR is just slightly positive and the much

higher frequency 89 GHz V-H is significantly negative, the preferentially oriented particles must be fairly small and not made up of larger dendrites.

4.2 September 12th, 2009

Late on the 12th of September, an easterly wind component behind a cold front led to the formation of discretely layered upslope clouds. Two light icing PIREPs were recorded within one hour and one-hundred nautical miles of the instrument location at CHILL. By 12:00Z, the Denver temperature sounding (Figure 13) had a freezing level at about 2km altitude and a nearly saturated profile above 1.5km that became saturated by 00Z on the 13th. The RHI reflectivity field (Figure 14) looking south at 185° azimuth from CHILL exhibits three distinct cloud layers – centered on 3.7km, 2km and 0.5km altitude. The vertical height scale of the reflectivity scale is matched up with the vertical scale of the temperature sounding for ease of
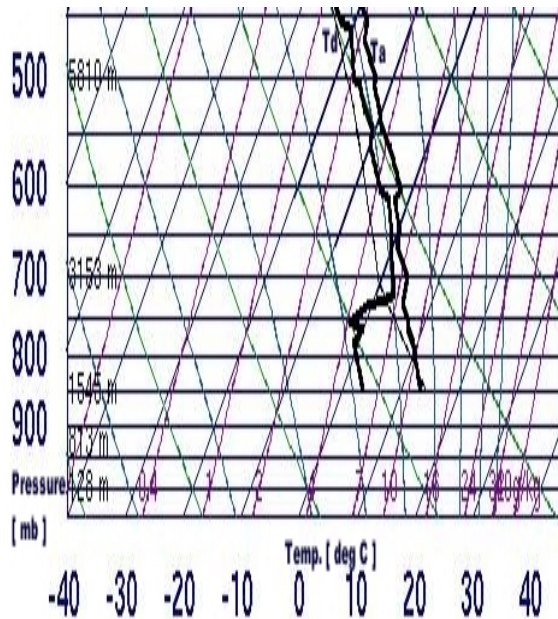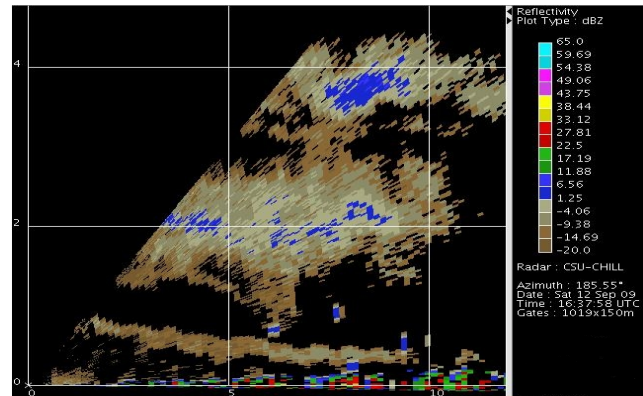

Figure 14. CHILL RHI view from 185° azimuth of reflectivity (b, [dBZ]) at 16:37Z on September 12th.

Figure 13. Atmospheric profile of ambient temperature (Ta) and dewpoint temperature (Td) from 12Z on September 12th from Denver, CO.
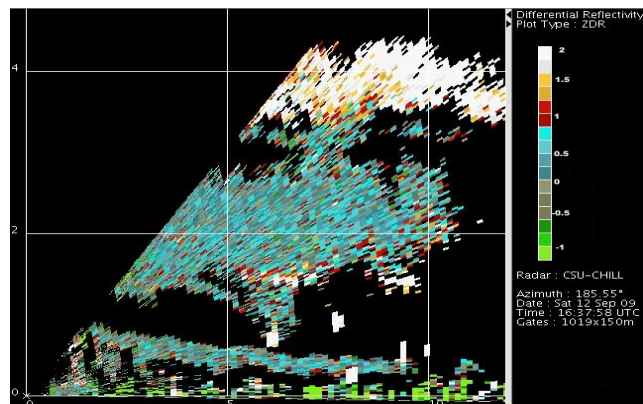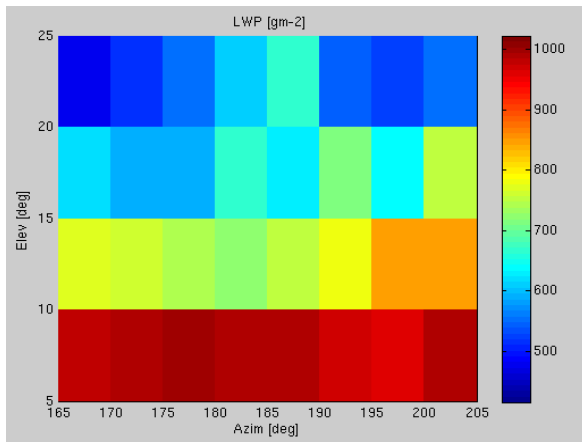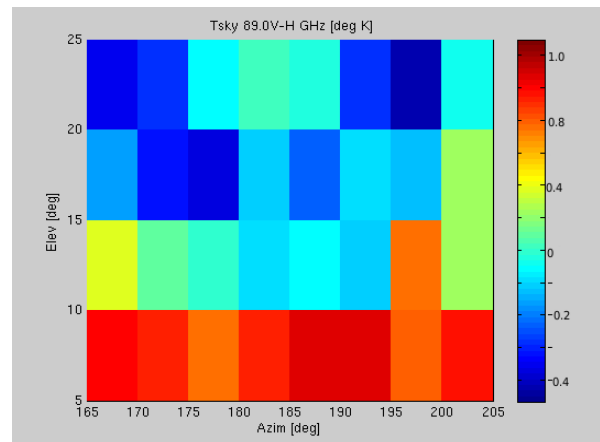

Figure 15. CHILL RHI views from 185° azimuth of differential reflectivity [dBZ] at 16:37Z on September 12th.

A)　　　　　**B)**

Figure 16.   NNMSR derived LWP (A, [gm^{-2}]), 89 GHz V-H (B, [^{o}K] at 16:37Z on September 12th.
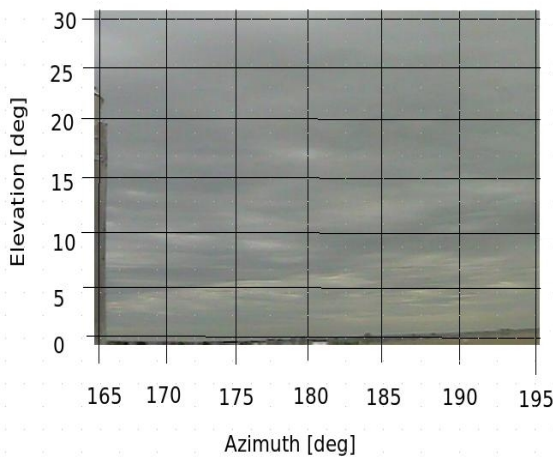

Figure 17.   Gridded visual sky sector image at 16:37 Z on September 12th.

comparison. All three layers offer only weak returns, with most values being below zero and only pockets of the upper layer reaching 6 dBZ. Analysis of the ZDR field (Figure 15a) leads to very interesting ramifications for the ability of satellite based detection methods to detect icing in this case. One can see that the lowest two layers have slightly positive ZDRs, indicating nearly round or axial-symmetric shapes of the reflectivity-weighted particle distribution.   The upper level, however, has a mean ZDR of about +2 dB.   This means that the dominant reflectivity-weighted hydrometeors in the volume are horizontally oriented. Significantly oriented particles at -15^{0}C must be plates or dendrites as opposed to oblate large raindrops, and since the layer reflectivity is so low the glaciated particles must be small and sparse.

On this day, the radiometer was collecting data every 5° azimuth and elevation with 1° resolution, which is why the image resolution (Figure 16a) seems reduced compared to the previous case study. The LWP field has discrete regions of relative maxima of about 350 gm^{-2} at elevations above 10°. Relative maxima in LWP spatially correspond to 89 V-H values near zero (Figure 16b), which is consistent with round particles. Other areas above 10° elevation have V-H values of -1 dB or below, which is consistent with oriented particles. The visual view of the sampled sky sector in Figure 17 shows a continuous grey stratiform cloud deck.

The important fact to note in this case is that satellite-based visible and infrared icing detection methods will sense only the glaciated upper layer of clouds and not be able warn for in-flight icing for the cloud layers lower down. Also, icing in multi-layer clouds are a very important scenario to detect since they can lead to sequenced icing events that can be more dangerous and unpredictable for controlled flight than icing from deeper single layered clouds. A ground-based system such as the NASA Icing Remote Sensing System, of which NNMSR will be a part, can efficiently detect the icing threat in the middle layer when positioned with a polarized S-band radar.

5. SUMMARY

The first purpose of this summer field program was to test the new, one-of-a-kind system for robustness and stability. After the two months of field testing and data collection, the scanhead drive and receivers seemed very stable.   The system was operated remotely in an automated fashion for most of the test period.

The second purpose of this study was to determine if the new NNMSR could aid in the detection of in-flight icing hazards. One case study time had multiple icing PIREPs located close to the instrumentation. Low radar reflectivity (<0 dBZ) indicated a lack of large reflectors. High radiometer LWP values and no preferred particle orientation were consistent with the presence of significant liquid drops aloft at a time with many positive icing PIREPs. At a later time with no reported PIREPs, high radar reflectivity (>10 dBZ) indicated the precence of large reflectors which are known to effectively scavenge available liquid drops.   Positive ZDR values meant

somewhat oriented particles. Low radiometer LWP values and a horizontal particle preference detected in the 89 GHz V-H signal were consistent with an all glaciated cloud and no icing PIREPs.

The second case study had three discrete cloud layers, the top of which was clearly glaciated based on the radar ZDR values. Two 'light' icing PIREPs were reported roughly at the height of the middle cloud layer. Satellite-based in-flight icing hazard warning systems, such as CIP, would not be able detect icing conditions in this case since they can only detect the highest cloud top. The NNMSR products were able to discern patchy relative maxima in LWP and 89 GHz V-H differences consistent with more round particles.

Based on the system's overall stability and ability to detect elevated LWP in association with icing verification from PIREPs, we have determined that the NNMSR would be a valuable addition to NIRSS for detecting in-flight icing hazards in the airport environment. This will especially be true in the coming years as the national network of S-band NEXRADs are upgraded to collect polarimetric moment data, as was available for this study at CSU's CHILL.

Future work includes more summer 2009 case analysis by averaging the CHILL moment data along the radar beam and comparing the results to radiometer LWP. Also, it might be useful to compare areal averaged GOES LWP product to radiometer LWP for the collected case studies. In 2010, the NNMSR will be positioned at NASA Glenn Research Center with NASA's Icing Remote Sensing System. Work will focus on applying the NIRSS algorithms with the NNMSR and NEXRAD data.

5. ACKNOWLEDGEMENTS

6. REFERENCES

Bernstein, B., McDonough, F., Politovich, M., Brown, B., Ratvasky, T., Miller, D., Wolff, C., and Cunning, G., "Current Icing Potential: Algorithm description and comparison to aircraft observations", *Journal of Applied Meteorology*, 44, pp. 969-986, 2005.

Fabry, F., and Meunier, V., "Conceptualisation and design of a Mesoscale Radiometer", *8th International Symposium on Tropospheric Profiling*, S06-P03-1, Delft, NL, 2009.

Lohnert, U., and S. Crewell, Accuracy of cloud liquid water path from ground-based microwave radiometry, 1, Dependency on cloud model statistics, *Radio. Sci.*, 38(3), 8041, 2003

Reehorst, A., Politovich, M., Zednik, S., Isaac, G., and Cober, S., "Progress in the development of practical remote detection of icing conditions", *Report NASA/TM-*2006-214242, 2006.

Serke, D. J., F. McDonough and M. Politovich, "Analysis of 3-D NEXRAD Mosaic Reflectivity Data Collocated with Research Aircraft and Satellite Data: Implications on In-Flight Icing". *13th Conference on Aviation, Range and Aerospace Meteorology Preprint*, New Orleans, LA, Jan 20-25, 2008.

Solheim, F., Godwin, J., Westwater, E., Han, Y., Keihm, S., Marsh, K., and Ware, R., "Radiometric profiling of temperature, water vapor and cloud liquid water using various inversion methods", *Radio Sci.*, **33**, pp. 393-404, 1998.

Troitsky, A.V., Osharin, A. M., Korolev, A. V., and Strapp, J. W., "Thermal Microwave Atmospheric Radiation Due to Scattering by Ice Particles in Clouds", *Journal of the Atmospheric Sciences*, 60, pp. 1608-1620, 2003.